Intramolecular energy transfer dynamics in 24-mode pyrazine by partitioning technique: A time-dependent approach

Cite as: J. Chem. Phys. **133**, 154111 (2010); https://doi.org/10.1063/1.3495953
Submitted: 18 July 2010 • Accepted: 11 September 2010 • Published Online: 19 October 2010

Ioannis Thanopulos, Paul Brumer and Moshe Shapiro

Intramolecular energy transfer dynamics in 24-mode pyrazine by partitioning technique: A time-dependent approach

Ioannis Thanopulos,[1,a] Paul Brumer,[2] and Moshe Shapiro[3]
[1]*Theoretical and Physical Chemistry Institute, National Hellenic Research Foundation, Athens 11635, Greece*
[2]*Department of Chemistry, Chemical Physics Theory Group, and Center of Quantum Information and Quantum Control, University of Toronto, Toronto, Ontario M5S 3H6, Canada*
[3]*Department of Chemistry and Department of Physics, The University of British Columbia, Vancouver V6T1Z1, Canada and Department of Chemical Physics, The Weizmann Institute, Rehovot 76100, Israel*

(Received 18 July 2010; accepted 11 September 2010; published online 19 October 2010)

We investigate the intramolecular energy transfer dynamics of the S_2 excited electronic state of pyrazine due to radiationless transitions to energetically lower-lying singlet electronic states using a new time-dependent method. The femtosecond decay of S_2 to the S_1 excited state and the picosecond decay of S_2 to the ground electronic state S_0 are studied within an efficient methodology for computing the intramolecular dynamics in multidimensional configurational spaces. Our method is based on partitioning the full configuration space into the (small) subspace of interest $\mathcal{Q}$ and the rest, the subspace $\mathcal{P}$. The exact equations of motion for the states in $\mathcal{Q}$, under the influence of $\mathcal{P}$, are derived in the time domain in form of a system of integrodifferential equations. Their numerical solution is readily obtained when the $\mathcal{Q}$ space consists of just a few states. Otherwise, the integrodifferential equations for the states in $\mathcal{Q}$ are transformed into a (larger) system of ordinary differential equations, which can be solved by a *single* diagonalization of a general complex matrix. The former approach is applied to study the pyrazine picosecond $S_2 \rightarrow S_0$ dynamics and the latter is applied to the study of the ultrafast pyrazine $S_2 \rightarrow S_1$ decay dynamics. © *2010 American Institute of Physics*. [doi:10.1063/1.3495953]

I. INTRODUCTION

The quantum mechanical treatment of intramolecular energy transfer dynamics in large molecules represents a challenging problem of fundamental importance. In particular, the energy transfer after photoinduced electronic excitations is in the center of current research in physical, life, and materials sciences.[1] Manifestations and uses of intramolecular electronic energy transfer are numerous. Some notable examples include control of chemical reactions,[2,3] light harvesting in photosynthesis,[4] design of high performance sensors,[5] molecular labeling,[6] and organic optoelectronic processes.[7]

Irrespective of whether solutions of the time-independent or the time-dependent Schrödinger equation are sought, the computational effort associated with the studies of intramolecular energy transfer grows exponentially with the number of nonseparable nuclear degrees of freedom. For this reason, techniques have been developed that allow one to focus on a specific configurational subspace of a molecule while taking into account its coupling to the rest of the dynamical space through effective matrix elements, with the Löwdin–Feshbach partitioning technique[8–11] being the most prominent among such methods in chemical physics.

In the past, the partitioning technique was primarily used as a starting point for further approximations that estimate system-environment effects. By contrast, recently, a time-independent partitioning technique was introduced for intramolecular dynamical calculations of large polyatomic molecules.[12] This method provides a useful tool for tackling the full quantum dynamics of large molecular systems. However, to include the study of active control on the intramolecular dynamics in (large) molecules would require the inclusion of time-dependent external interactions, as, e.g., laser fields.[2,3,13] For this reason, we have developed a time-dependent partitioning technique that can be used for efficient intramolecular dynamics computations of large polyatomic molecules subject to external time-dependent interactions. The first applications of this method to small systems were reported recently.[14]

In this work, we apply the time-dependent partitioning technique to the photophysics of a larger system, that of the pyrazine ($C_4H_4N_2$) molecule. Of particular long standing interest has been the ultrafast dynamics following the optical excitation of pyrazine from the ground state $S_0(^1A_g)$ to the second excited singlet state $S_2(^1B_{2u})$ and the dynamics of internal conversion (IC) from the S_2 to the $S_1(^1B_{3u})$ first excited singlet state and to the S_0 state.[15–20]

This paper is organized as follows. Section II describes the theory for the time-dependent partitioning technique. The 24-dimensional pyrazine model is reviewed in Sec. III. The results of our investigation of the IC dynamics of $S_2 \rightarrow S_1$ and

[a]Electronic mail: ithano@eie.gr.

$S_2 \rightarrow S_0$ IC in pyrazine within the time-dependent partitioning technique are presented in Sec. IV. We conclude in Sec. V.

II. THEORY

The objective here is to develop an efficient method for computing the quantum dynamics of a set of relatively small number of "interesting" states, belonging to subspace $\mathcal{Q}$, that are coupled to a much larger set of "less-interesting" states, belonging to a (prediagonalized) subspace $\mathcal{P}$. Such an approach is necessary because a full dimensionality treatment incorporating all states in $\mathcal{Q} \oplus \mathcal{P}$ is, in general, not feasible due to the formidable size of $\mathcal{P}$.

We start the formal development by considering the Hamiltonian H on the entire Hilbert space $\mathcal{H}=\mathcal{Q} \oplus \mathcal{P}$. We define as H_Q and H_P the Hamiltonian of the subspaces $\mathcal{Q}$ and $\mathcal{P}$, respectively, such that $Q+P=1$. The set of states in $\mathcal{Q}$ obeys the Q-projected $(\mathcal{E}_\ell - H_Q)|\ell\rangle = 0$ $(\ell = 1, \ldots, q)$ equation, whereas the set of states in $\mathcal{P}$ obeys the P-projected equation $(E^- - H_P)|E, n^-\rangle = 0$. Here, the subspace $\mathcal{P}$ is assumed to be dense and well approximated by a continuum or a quasicontinuum of eigenenergies. The index n denotes all quantum numbers other than the energy E, and $E^- \equiv E - i\epsilon$; we use ("minus") boundary conditions for the scattering solutions that correlate with a single freely moving state in the $\mathcal{P}$ space when the scattering process is over. Defining $V_{QP} \equiv QHP$ and $H - H_Q - H_P = V_{QP} + V_{PQ}$ for the interaction in H between the two spaces, the Hamiltonian matrix H for the entire Hilbert space $\mathcal{H}$ can be written in a matrix form as

$$\mathsf{H} = \begin{pmatrix} \mathsf{H_Q} & \mathsf{V_{QP}} \\ \mathsf{V_{QP}^\dagger} & \mathsf{H_P} \end{pmatrix}. \tag{1}$$

We note that in the above only the submatrices $\mathsf{H_Q}$ and $\mathsf{H_P}$ are diagonal.

It is possible to solve the dynamics in the entire $\mathcal{H}$ space by expanding Ψ, the solution of the time-dependent Schrödinger equation expressed in atomic units $(\hbar = 1)$ as $i\dot{\Psi} = H\Psi$, as

$$|\Psi(t)\rangle = \sum_{\ell=1}^{q} b_\ell(t) e^{-i\mathcal{E}_\ell t} |\ell\rangle + \int dE b_{E,n}(t) e^{-iEt} |E, n^-\rangle. \tag{2}$$

Substituting Eq. (2) into the time-dependent Schrödinger equation gives a set of ordinary differential equations,

$$\dot{b}_\ell(t) = i \int dE b_{E,n}(t) \mathcal{V}(\ell|E,n) e^{-i(E-\mathcal{E}_\ell)t}, \quad \ell = 1, \ldots, q, \tag{3}$$

$$\dot{b}_{E,n}(t) = i \sum_{k=1}^{q} b_k(t) \mathcal{V}^*(k|E,n) e^{i(E-\mathcal{E}_k)t} \quad \text{for every } E, \tag{4}$$

with $\mathcal{V}(k|E,n) \equiv \langle k|V_{QP}|E, n^-\rangle$; in general, the $\mathcal{V}(k|E,n)$ quantities can be computed, numerically or analytically, after the eigenstates in the $\mathcal{Q}$ and $\mathcal{P}$ spaces have been obtained. These equations cannot be readily solved because of the huge number of "bath" coefficients $b_{E,n}(t)$ appearing in Eq. (4). We can, however, formally eliminate Eq. (4) by integrating them over time and substituting the resulting expressions into Eq. (3) to obtain

$$\dot{b}_\ell(t) = i \int dE b_{E,n}(0) \mathcal{V}(\ell|E,n) e^{-i(E-\mathcal{E}_\ell)t} + \sum_{k=1}^{q} e^{-i(\mathcal{E}_k - \mathcal{E}_\ell)t} \int_0^t dt' b_k(t') F_{\ell,k}(t-t'), \tag{5}$$

where

$$F_{\ell,k}(\tau) \equiv i e^{i\mathcal{E}_k \tau} \int dE \sum_n \mathcal{V}(\ell|E,n) \mathcal{V}^*(k|E,n) e^{-iE\tau}, \tag{6}$$

with $\tau \equiv t - t'$.

The correlation functions $F_{\ell,k}(\tau)$ of Eq. (6) can be expanded to the desired accuracy as a sum of exponentials,

$$F_{\ell,k}(\tau) = i \exp(i\mathcal{E}_k \tau) \sum_{\lambda=1}^{M} W_\lambda^{\ell,k} e^{-i\Omega_\lambda \tau - G_\lambda |\tau|/2}. \tag{7}$$

As in most finite fitting procedures, the set of fitting parameters $\{W_\lambda^{\ell,k}, \Omega_\lambda, G_\lambda\}$ is not unique. This, however, need not detract from the quality of representation of $F_{\ell,k}(\tau)$, the goodness of which can be monitored by comparing $F_{\ell,k}(\tau)$ obtained via Eq. (7) with the correlation functions obtained by directly integrating Eq. (6).

The expansion of $F_{\ell,k}(\tau)$ as a sum of exponentials allows one to transform the integrodifferential equations of Eq. (5) into a set of ordinary differential equations. We obtain that

$$\dot{b}_\ell(t) = i K_\ell^0(t) + i \sum_{\lambda=1}^{M} \exp[i(\mathcal{E}_\ell - \Omega_\lambda)t] \mathcal{J}_\lambda^\ell(t), \tag{8}$$

with

$$\mathcal{J}_\lambda^\ell(t) = i \sum_{k=1}^{q} W_\lambda^{\ell,k} \exp(-G_\lambda t/2) \times \int_0^t dt' b_k(t') \exp[-i(\mathcal{E}_k - \Omega_\lambda + iG_\lambda/2)t'] \tag{9}$$

and

$$K_\ell^0(t) = \exp(i\mathcal{E}_\ell t) \int dE b_{E,n}(0) \mathcal{V}(\ell|E,n) \exp(-iEt). \tag{10}$$

Rather than using Eq. (9) directly, we note that the $\mathcal{J}_\lambda^\ell(t)$ "effective-mode"[21] amplitudes satisfy a set of first order differential equations,

$$\dot{\mathcal{J}}_\lambda^\ell(t) = \frac{i}{2} G_\lambda \mathcal{J}_\lambda(t) + i \sum_{k=1}^{q} W_\lambda^{\ell,k} b_k(t) e^{-i(\mathcal{E}_k - \Omega_\lambda)t}. \tag{11}$$

Thus, we have transformed the q integrodifferential equations of Eq. (5) into a set of $q \times (M+1)$ ordinary differential equations given by Eqs. (8)–(11).

Denoting $\tilde{b}_k(t) \equiv \exp(-i\mathcal{E}_k t) b_k(t)$ and $\tilde{\mathcal{J}}_\lambda^\ell(t) \equiv \exp(-i\Omega_\lambda t) \mathcal{J}_\lambda^\ell(t)$, we obtain our working equations,

$$\dot{\mathbf{c}}(t) = i\mathcal{K} \cdot \mathbf{c}(t) + i\mathbf{K}^0(t), \tag{12}$$

where $\mathbf{c}(t) = (\tilde{b}_1, \ldots, \tilde{b}_q, \tilde{\mathcal{J}}_1^1, \ldots, \tilde{\mathcal{J}}_M^1, \ldots, \tilde{\mathcal{J}}_1^q, \ldots, \tilde{\mathcal{J}}_M^q)^\mathsf{T} \equiv (\tilde{b}_1, \ldots, \tilde{b}_N, \tilde{\mathcal{J}}^{(1)}, \ldots, \tilde{\mathcal{J}}^{(qM)})^\mathsf{T}$, with all $\tilde{\mathcal{J}}^{(i)}(0) = 0$, and $\mathbf{K}^0(t) = (K_1^0, \ldots, K_q^0, 0, \ldots, 0)^\mathsf{T}$. Here, the superscript T is the

transpose operation and $\mathcal{K}$ is a time-independent complex matrix, with a characteristic block structure, given by

$$\mathcal{K}=\begin{pmatrix}\mathcal{S} & \mathcal{Y}\\ \mathcal{Z} & \mathcal{R}\end{pmatrix},\quad \mathcal{Z}=\begin{pmatrix}\mathsf{W}^{(1)}\\ \cdots\\ \mathsf{W}^{(qM)}\end{pmatrix},\quad \mathcal{Y}=\begin{pmatrix}\Omega^{(1)}\\ \cdots\\ \Omega^{(q)}\end{pmatrix}. \tag{13}$$

In Eq. (13), $\mathcal{S}_{k,k'}=\delta_{k,k'}\mathcal{E}_k$ and $\mathcal{R}_{i,i'}=\delta_{i,i'}(\Omega_\lambda+iG_\lambda/2)$ for the diagonal blocks. The $\mathsf{W}^{(i)}$ rows of matrix $\mathcal{Z}$ are defined as $\mathsf{W}^{(i)}=(W_\lambda^{\ell,1},\ldots,W_\lambda^{\ell,q})$, and the $\Omega^{(i)}$ rows of matrix $\mathcal{Y}$ are defined as $[\Omega^{(i)}]_{k,j}=1$ for $k+(i-1)\times M\le j\le k+i\times M$, and $[\Omega^{(i)}]_{k,j}=0$ otherwise. Here, $k,k'=1,\ldots,q$, $j=1,\ldots,q\times M$, and $i,i'=\lambda+(\ell-1)\times M$, with $\lambda=1,\ldots,M$ forming the inner loop and $\ell=1,\ldots,q$ forming the outer loop.

Given these definitions, we write the solution of Eq. (12) as

$$\mathbf{c}(t)=\sum_j^{M'}\mathbf{\Lambda}_j e^{i\lambda_j t}\left(c_j^0-i\int_0^t dt'[\mathsf{L}^{-1}\cdot\mathbf{K}^0(t')]_j e^{-i\lambda_j t'}\right), \tag{14}$$

where $M'=q\times(M+1)$ is the number of λ_j eigenvalues and $\mathbf{\Lambda}_j$ eigenvectors of $\mathcal{K}$. The columns of the $\mathsf{L}\equiv[\mathbf{\Lambda}_1,\ldots,\mathbf{\Lambda}_{M'}]$ matrix are the eigenvectors of $\mathcal{K}$, and $[\mathsf{L}^{-1}\cdot\mathbf{K}^0(t)]_j$ are the jth column vector of the $\mathsf{L}^{-1}\cdot\mathbf{K}^0(t)$ matrix. The vector of complex coefficients c_j^0 is given as $\mathbf{c^0}=\mathsf{L}^{-1}\cdot\mathbf{c}(0)$. We note that since $\mathcal{K}$ is not Hermitian, $\mathsf{L}^{-1}\neq\mathsf{L}^\dagger$.

In the quasicontinuum case, the spectrum of H_P is made up of p discrete eigenvalues $(\mathcal{E}_\beta-H_P)|\beta\rangle=0$. In that case, we equate the states $|E,n^-\rangle$ with vanishingly narrow resonances in the $\mathcal{P}$ space. In the following sections, we apply the methodology described above to the $S_2\to S_1$ and $S_2\to S_0$ energy transfer dynamics in pyrazine, a case of considerable interest.

III. THE PYRAZINE MODEL

We consider internal conversion using the full 24-mode model of pyrazine by Raab *et al.*[15] The pyrazine molecule is modeled by normal modes, coupled by terms represented as polynomials, whose coefficients are made to fit the *ab initio* calculations. The Hamiltonian of the system is given by

$$H=\begin{pmatrix}H_{S_2}(q_1,\ldots,q_{24}) & V^{S_2S_1}(q_1,\ldots,q_{24})\\ V^{S_2S_1}(q_1,\ldots,q_{24}) & H_{S_1}(q_1,\ldots,q_{24})\end{pmatrix}, \tag{15}$$

with

$$H_s(q_1,\ldots,q_{24})=\sum_{i=1}^{24}\frac{\omega_i}{2}\left(\frac{\partial^2}{\partial q_i^2}+q_i^2\right)+\sum_{i\in G_1}a_i^s q_i+\sum_{i,j\in G_2}a_{ij}^s q_i q_j\mp\Delta,\quad s=S_2,S_1, \tag{16}$$

$$V^{S_2S_1}(q_1,\ldots,q_{24})=\lambda_{10a}q_{10a}+\sum_{i,j\in G_4}c_{ij}q_i q_j, \tag{17}$$

where ω_i are the normal mode frequencies of the ground electronic state S_0 of pyrazine, 2Δ is the energy difference between the S_2 and the S_1 electronic surfaces, a_i^s and $a_{i,j}^s$ are the coupling constants within the surface k for $k=S_2,S_1$, and λ_{10a} and c_{ij} are the coupling terms between the S_2 and the S_1 electronic surfaces. We further denote by G_1 the set of normal modes that have A_g symmetry, by G_2 the set of normal modes that have the same symmetry, and by G_4 all pairs of modes, whose product is of B_{1G}.

We can obtain the vibrational eigenstates on the decoupled S_2 and S_1 surfaces after diagonalization of the H_{S_2} and H_{S_1} Hamiltonians, as described in Ref. 12. We define the $\mathcal{Q}$ subspace to be composed of the 176 vibrational eigenstates of the S_2 electronic state that have the largest Franck–Condon overlap with the ground vibrational state of the S_0 electronic state. Furthermore, we define the $\mathcal{P}$ subspace as the set of vibrational eigenstates in S_1 with energy up to 1.6 eV. The same $\mathcal{P}$ space is used for the $S_2\to S_0$ dynamics, in a purely phenomenological fashion, as described below, while the $S_2\to S_0$ model used is rather artificial and primarily serves the purpose of applying our method on a different parameter set.

In the eigenstate basis defined by the set including the states in $\mathcal{Q}$ and $\mathcal{P}$, the matrix of the Hamiltonian given by Eq. (15) takes the block form of Eq. (1). We now apply the methodology presented in Sec. II to the IC dynamics of the S_2 state to the S_1 and S_0 states in pyrazine. Our results are discussed in Sec. IV.

Lastly, we note that in this work we apply our method on intramolecular dynamics between two electronic states of the pyrazine molecule. Nevertheless, the methodology presented is not limited to any number of electronic states as long as one can divide the total number of states in interesting states to be monitored, the states in $\mathcal{Q}$, and dynamically less-interesting states, the states in $\mathcal{P}$.

IV. THE $S_2\to S_1$ AND $S_2\to S_0$ IC DYNAMICS IN PYRAZINE

The first step for calculating the dynamics according to Eq. (12) is the calculation of the correlation functions $F_{\ell,k}(\tau)$ $(\ell,k=1,\ldots,q)$, as defined in Eq. (6). This task can be daunting in the case of a large polyatomic molecule, such as pyrazine, since the number of states M in the $\mathcal{P}$ space is usually very large, and therefore the computation of q^2 correlation functions becomes computationally very time-consuming. Fortunately, the computation of the correlation functions can be significantly accelerated by the application of coarse-graining in the $\mathcal{P}$ space.

A. Coarse-graining in the $\mathcal{P}$ space

The calculation of the correlation functions in our case pertains to computing

$$F_{\ell,k}(t)\equiv ie^{i\mathcal{E}_k t}\sum_{n=1}^{M'}\mathcal{W}_n^{\ell,k}e^{-iE_n t}\equiv ie^{i\mathcal{E}_k\tau}f_{\ell,k}(t), \tag{18}$$

with $\mathcal{W}_n^{\ell,k}\equiv\langle\ell|V^{S_2S_1}|n\rangle\langle n|V^{S_2S_1}|k\rangle$, for $|\ell\rangle,|k\rangle\in\mathcal{Q}$, $|n\rangle\in\mathcal{P}$, where $\ell,k=1,\ldots,176$ and $n=1,\ldots,M'$, with $M'\approx 12\,500\,000$.

In order to speed up this task computationally, we coarse-grain the $\mathcal{P}$ space by dividing the energy range up to 1.6 eV in N_{bins} equally spaced energy intervals (bins). To each bin, we assign the energy E_s $(s=1,\ldots,N_{\text{bins}})$, defined by the energy of its midpoint, and the $\tilde{\mathcal{W}}_s^{\ell,k}$ value defined as

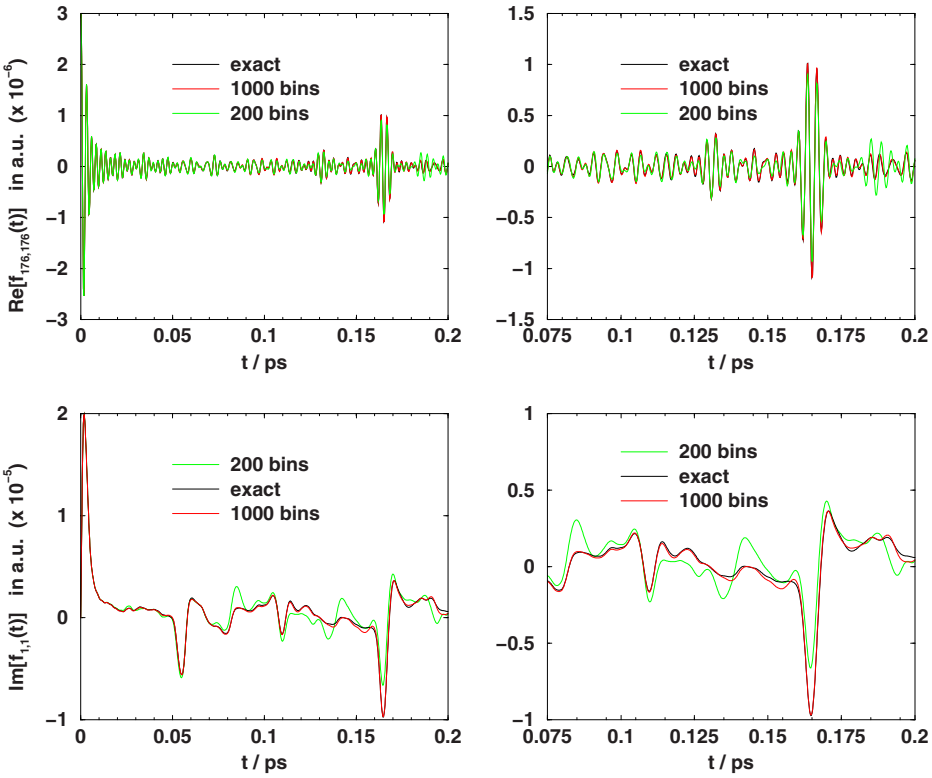

FIG. 1. Exact vs coarse-grained correlation functions using 200 and 1000 bins. (Upper panels) The real part of the autocorrelation function corresponding to state $|176\rangle$ in $\mathcal{Q}$ during the first 200 fs (left panel) and the same over a magnified 75–200 fs time interval (right panel). (Lower panels) The imaginary part of the autocorrelation function corresponding to state $|1\rangle$ in $\mathcal{Q}$ during the first 200 fs (left panel) and the same over a magnified 75–200 fs time interval (right panel).

$$\tilde{W}_s^{\ell,k} = \frac{\Sigma_{i=1}^{M_s} W_i^{\ell,k}}{M_s}, \tag{19}$$

where M_s is the number of states in $\mathcal{P}$ with energy within the energy range of the sth bin.

In Fig. 1, we show the autocorrelation functions during the first 200 fs for the energetically lowest and highest states in $\mathcal{Q}$, $|1\rangle$ and $|176\rangle$, respectively, obtained by the application of coarse-graining in the $\mathcal{P}$ space using 200 and 1000 bins. In the same figure, we also show the exact, i.e., without coarse-graining in $\mathcal{P}$, autocorrelation function for the $|1\rangle$ and $|176\rangle$ states. More specifically, in the left panels of Fig. 1, the real part of $f_{176,176}(t)$ (upper) and the imaginary part of $f_{1,1}(t)$ (lower) for the first 200 fs are presented, while the right panels focus on the 75–200 fs time interval for the same autocorrelation functions. Evidently, the coarse-graining with 200 bins is insufficient for correct representation of the autocorrelation functions. On the other hand, as shown in Fig. 1, using 1000 bins results in autocorrelation functions that are practically indistinguishable from the exact one, independently of the energy of the state in the $\mathcal{Q}$ space. The application of coarse-graining works equally well for the cross-correlation functions (not shown here) as for the autocorrelation functions. We note that the calculation of 176×176 correlation functions for the first 200 fs using 1000 bins in the $\mathcal{P}$ space requires 1.5 CPU hours on a single processor, which is a factor of 1000 faster than the CPU time required for calculating the exact correlation functions on the same processor.

B. Fitting the correlation functions to a sum of exponential terms

The second step in the calculation according to Eq. (12) is the expression of the correlation functions $f_{\ell,k}(t)$ as a sum of M exponential terms, as given by Eq. (7). Here, we choose M equidistant energy values in the 0–1.6 eV range and calculate for each energy E_λ $(\lambda = 1, \ldots, M)$ the corresponding $W_\lambda^{\ell,k}$ $(\lambda = 1, \ldots, M)$ as the complex coefficients of the analytic Fourier transform of the $f_{\ell,k}(t)$ correlation function at energy E_λ.

In Fig. 2, we compare the exact autocorrelation functions

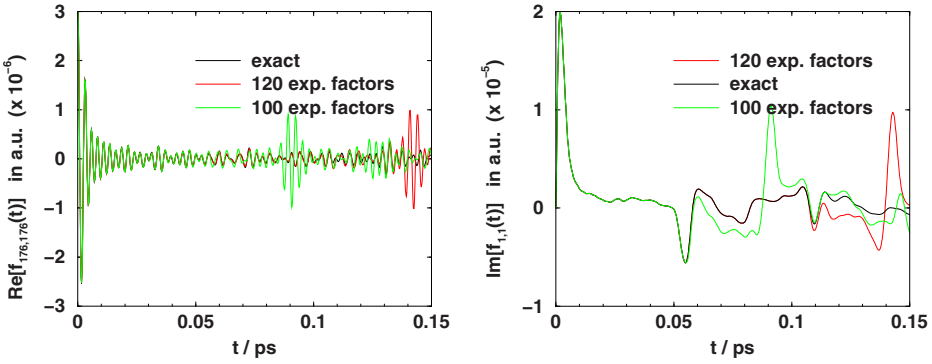

FIG. 2. Exact vs fitted autocorrelation functions with 100 and 120 exponential terms: (Left panel) The real part of $f_{176,176}(t)$. (Right panel) The imaginary part of $f_{1,1}(t)$.

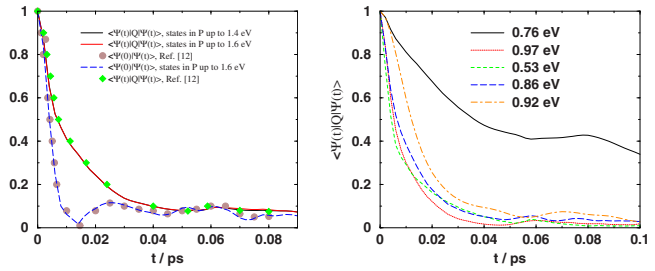

FIG. 3. Decay dynamics for various initial vibrational states of the S_2 electronic state. (Left panel) The $\langle\Psi(0)|\Psi(t)\rangle$ and the $\langle\Psi(t)|\mathcal{Q}|\Psi(t)\rangle$ dynamics of the initial superposition state used in Ref. 12 obtained with our methodology, where the S_1 space includes vibrational states up to 1.4 and 1.6 eV. (Right panel) The $\langle\Psi(t)|\mathcal{Q}|\Psi(t)\rangle$ dynamics for the initial $|1\rangle$ (0.53 eV), $|16\rangle$ (0.76 eV), $|32\rangle$ (0.86 eV), $|46\rangle$ (0.92 eV), and $|64\rangle$ (0.97 eV) states in the S_2 space.

for states $|1\rangle$ and $|176\rangle$ in $\mathcal{Q}$ to the fitted functions with 100 and 120 exponential terms. The left panel depicts the real part of $f_{176,176}(t)$ and the right panel depicts the imaginary part of the $f_{1,1}(t)$ function. We find that at least 120 terms are needed for a sufficient representation of the exact correlation functions for the first 100 fs, which is the time interval that we are interested in. As shown in Fig. 2, the fitting procedure with 120 exponential terms works equally well for the real and imaginary parts of the autocorrelation functions (and the cross-correlation functions—not shown here), independently of the energy of the state in $\mathcal{Q}$.

C. The $S_2 \rightarrow S_1$ decay

The $S_2 \rightarrow S_1$ is widely regarded as a model for fast internal conversion. Typical time scales are of the order of 20 fs.[12] Here, we calculate this internal conversion dynamics in accord with Eq. (12). For this purpose, we diagonalize the general complex matrix $\mathcal{K}$ of dimension $q \times (M+1)$, with $q=176$ and $M=120$, and subsequently calculate the inverse eigenvector matrix of $\mathcal{K}$. These tasks, performed using standard LAPACK/BLAS routines, require in total 120 CPU hours on a single processor.

In Fig. 3, we present the decay dynamics for various initial vibrational states of the S_2 space. In the right panel, we consider the time evolution of the $\mathcal{Q}$-space population $\langle\Psi(t)|\mathcal{Q}|\Psi(t)\rangle$ when the initial population in the S_2 space is on a single state; the decay for the $|1\rangle$ (0.53 eV), $|16\rangle$ (0.76 eV), $|32\rangle$ (0.86 eV), $|46\rangle$ (0.92 eV), and $|64\rangle$ (0.97 eV) states is depicted. In the left panel, the $\mathcal{Q}$-space population dynamics, when the S_1 space includes vibrational states up to 1.4 eV and up to 1.6 eV, and the $\langle\Psi(0)|\Psi(t)\rangle$ dynamics, including S_1 vibrational states up to 1.6 eV, for the initial superposition state used in Ref. 12 are shown; the agreement with the results of Ref. 12 is excellent.

The results in the left panel of Fig. 3 are in good agreement with the corresponding pyrazine results obtained by the multiconfigurational time-dependent Hartree (MCTDH) method.[15,22] As discussed in detail in Ref. 12, the differences of our results from the MCTDH results are due to the fact that the initial state in S_2 used in this work, as well as in Ref. 12, overlaps by about 80% with the initial state used in the MCTDH calculations.[12] Achieving 100% overlap between the two initial vectors would require to include a much larger number of states in the $\mathcal{Q}$ space used here since the convergence to full overlap is very slow after the first 176 states in S_2 with the largest Franck–Condon factors to the ground vibrational state of S_0 have been included in the $\mathcal{Q}$ space.[12]

The IC decay dynamics from the S_2 to the S_1 surface in pyrazine occurs within the first 100 fs. The present method is evidently capable of capturing the ultrafast intramolecular energy transfer dynamics in a polyatomic molecule, such as pyrazine.

D. The $S_2 \rightarrow S_0$ decay

The $S_2 \rightarrow S_0$ decay occurs in a much longer time scale than does the $S_2 \rightarrow S_1$ decay and hence presents a greater challenge to time-dependent methods. Here, the decay of the ground vibrational state of S_2 into the S_0 manifold of states, which occurs in $\approx$13 ps,[18,19,23] has been poorly studied computationally. Also, little information is available about the couplings between the electronic states. Therefore, we model the $S_2 \rightarrow S_0$ decay by an *ad hoc* scaling of the coupling between the S_2 and S_1 surfaces given by Eq. (17) by a factor $\sqrt{s}$. The effect of scaling on the coupling between S_2 and S_1 by $\sqrt{s}$ results in a corresponding scaling of the correlation functions $f_{\ell,k}(t)$ by a factor of s. The scaled correlation functions $\tilde{f}^s_{\ell,k}(t) \equiv f_{\ell,k}(t)/s$ are then used in the $S_2 \rightarrow S_0$ IC dynamics calculation. As in the case of the $S_2 \rightarrow S_1$ decay dynamics, we include here all eigenstates with energy up to 1.6 eV in the $\mathcal{P}$ space, which proved to be sufficient with respect to the convergence of the computed correlation functions of all states in $\mathcal{Q}$. However, we consider all correlation functions only up to $t=4$ ps. After that time, these functions show dubious recurrences. The recurrences remain even when we expand the $\mathcal{P}$ space by about 40%, reaching our limits with respect to the available computational resources. Nevertheless, we expect that these recurrences are unphysical and their presence is due to the density of states within our model, which is probably too low for the correct description of the dynamics beyond 4 ps.

We first determine the value of s that gives $\tau=13$ ps for state $|1\rangle$ in S_2. For this purpose, we calculate the decay dynamics of $|1\rangle$ for various s values and, for each s value, we obtain a τ by fitting a single exponential decay function $\exp(-t/\tau)$ to the calculated dynamics for the first 4 ps, the first unrealistic recurrence in the $\tilde{f}_{1,1}(t)$ correlation function occurring at $\approx$3 ps. The τ values from the fitting, with the error bars at the 95% confidence level, are given in the left panel of Fig. 4; we find that $s=1500$ gives $\tau \approx 13$ ps. Note that the dynamics for each s value is obtained by solving the integrodifferential equation for state $|1\rangle$ in S_2, as defined in Eq. (5), where the first term in Eq. (5) is absent here since the S_0 space is assumed initially empty.

As an example of the $S_2 \rightarrow S_0$ dynamics, we calculate the decay dynamics for the $|16\rangle$ (0.76 eV), $|32\rangle$ (0.86 eV), $|46\rangle$ (0.92 eV), and $|64\rangle$ (0.97 eV) initial states in S_2 by solving the corresponding integrodifferential equation [Eq. (5)] for each state using $s=1500$. We restrict our calculations to the first 5 ps in order to avoid the unrealistic recurrences in the autocorrelation functions for times beyond the first few pico-

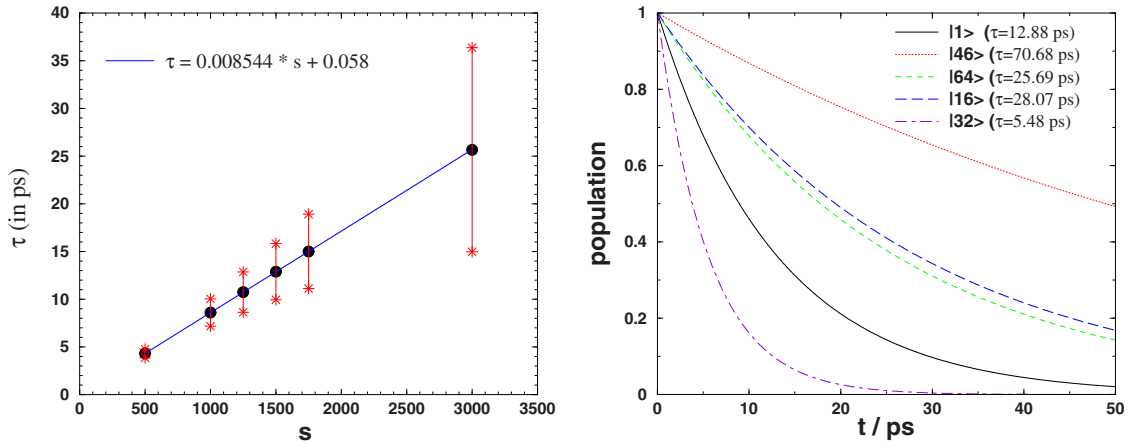

FIG. 4. The $S_2 \rightarrow S_0$ decay. (Left panel) The decay rate τ of the ground vibrational state in $S_2|1\rangle$ for various values of s. (Error bars at the 95% confidence level). (Right panel) Exponential decay with $s=1500$ for states $|1\rangle$ (0.53 eV), $|16\rangle$ (0.76 eV), $|32\rangle$ (0.86 eV), $|46\rangle$ (0.92 eV), and $|64\rangle$ (0.97 eV) in S_2.

seconds. The calculated decay dynamics for each of the above states is then used to fit an exponential decay $\exp(-t/\tau_i)$ for each state $|i\rangle$ $(i=1,16,32,46,64)$. In the right panel of Fig. 4, we present the exponential decay up to 50 ps for these states using the corresponding $\tau_1=12.88$ ps, $\tau_{16}=28.07$ ps, $\tau_{32}=5.48$ ps, $\tau_{46}=70.68$ ps, and $\tau_{64}=25.69$ ps, τ-values obtained from the fitting procedure. The resultant curves display a wide range of decay times, from extremely long (for $|46\rangle$) to relatively short (for $|32\rangle$). These results should motivate experimental studies to better map out the couplings between the S_2 and the S_0 surfaces that result in these long time IC dynamics.

V. CONCLUSION

We have computed the IC dynamics of the S_2 excited electronic state of pyrazine to all energetically lower-lying singlet electronic states using a newly developed time-dependent procedure. Two different computational methods were considered for two different transitions. The femtosecond decay $S_2 \rightarrow S_1$ and the picosecond decay of S_2 to the ground electronic state S_0 were investigated within an efficient methodology for computing the intramolecular energy transfer dynamics in multidimensional configurational spaces. The method is based on partitioning the full configuration space into the (small) subspace of interest $\mathcal{Q}$ and the rest, the subspace $\mathcal{P}$. The exact equations of motion for the states in $\mathcal{Q}$, under the influence of $\mathcal{P}$, are derived in the time domain in form of a system of integrodifferential equations. Their numerical solution is readily obtained when the $\mathcal{Q}$ space is consisting of just a few states. Otherwise, the integrodifferential equations for the states in $\mathcal{Q}$ are transformed into a (larger) system of ordinary differential equations, which can be solved by a *single* diagonalization of a general complex matrix. The former approach is applied to the investigation of the picosecond $S_2 \rightarrow S_0$ energy transfer dynamics and the latter is applied to the study of the ultrafast $S_2 \rightarrow S_1$ decay dynamics. This methodology allows for the calculation of intramolecular energy transfer dynamics in polyatomic molecules. Due to its formulation in the time domain, this method can be easily extended to include external time-dependent interactions, as laser pulses—the subject of a future work.

ACKNOWLEDGMENTS

I.T. acknowledges the financial support from the EU-FP7 IRG PIRG03-GA-2008-230943 (COPET) program. M.S. and P.B. acknowledge support from NSERC and NSF (Grant No. CHE-0848198). M.S. acknowledges support from the U.S. DoD DTRA project as well as support from UBC's Peter Wall Institute for Advanced Studies.

[1] V. May and O. Kühn, *Charge and Energy Transfer Dynamics in Molecular Systems: A Theoretical Introduction* (Wiley-VCH, Berlin, 2000).
[2] M. Shapiro and P. Brumer, *Principles of Quantum Control of Molecular Processes* (Wiley-Interscience, New York, 2003).
[3] S. A. Rice and M. Zhao, *Optical Control of Molecular Dynamics* (Wiley, New York, 2000).
[4] G. R. Fleming and G. D. Scholes, Nature (London) **431**, 256 (2004); E. Collini, K. E. Wilk, P. M. G. Curnmi, P. Brumer, and G. D. Scholes, *ibid.* **463**, 644 (2010).
[5] S. M. Borisov and O. S. Wolfbeis, Chem. Rev. (Washington, D.C.) **108**, 423 (2008).
[6] B. Valeur, *Molecular Fluorescence: Principles and Applications* (Wiley-VCH, New York, 2002).
[7] J. Zheng, P. R. Nicovich, and R. M. Dickson, Annu. Rev. Phys. Chem. **58**, 409 (2007).
[8] U. Fano, Nuovo Cimento **12**, 156 (1931); Phys. Rev. **124**, 1866 (1961).
[9] H. Feshbach, Ann. Phys. (N.Y.) **5**, 357 (1958).
[10] P. O. Löwdin, J. Math. Phys. **3**, 969 (1962); J. Mol. Spectrosc. **10**, 12 (1963).
[11] M. Shapiro, J. Chem. Phys. **56**, 2582 (1972); J. Phys. Chem. **102**, 9570 (1998).
[12] P. S. Christopher, M. Shapiro, and P. Brumer, J. Chem. Phys. **124**, 184107 (2006).
[13] D. J. Tannor, *Introduction to Quantum Mechanics: A Time Dependent Perspective* (University Science Press, Sausalito, 2007).
[14] I. Thanopulos, P. Brumer, and M. Shapiro, J. Chem. Phys. **129**, 194104 (2008).
[15] A. Raab, G. A. Worth, H.-D. Meyer, and L. S. Cederbaum, J. Chem. Phys. **110**, 936 (1999); G. A. Worth, H.-D. Meyer, and L. S. Cederbaum, *ibid.* **105**, 4412 (1996).
[16] S. Krempl, M. Winterstetter, H. Plöhn, and W. Dömcke, J. Chem. Phys. **100**, 926 (1994); G. Stock and W. Dömcke, *ibid.* **97**, 12446 (1993); G. Stock, C. Woywood, W. Dömcke, T. Swinney, and B. S. Hudson, *ibid.* **103**, 6851 (1995).
[17] P.S. Christopher, M. Shapiro, and P. Brumer, J. Chem. Phys. **123**, 064313 (2005); **125**, 124310 (2006).

[18] R. Islampour and M. Miralinaghi, J. Phys. Chem. A **113**, 2340 (2009).
[19] V. Stert, P. Farmanara, and W. Radloff, J. Chem. Phys. **112**, 4460 (2000).
[20] X. S. Chen and V. S. Batista, J. Chem. Phys. **125**, 124313 (2006).
[21] B. M. Garraway, Phys. Rev. A **55**, 4636 (1997); B. J. Dalton and B. M. Garraway, *ibid.* **68**, 033809 (2003); L. Mazzola, S. Maniscalco, J. Piilo, K.-A. Suominen, and B. M. Garraway, *ibid.* **80**, 012104 (2009).
[22] I. Burghardt, K. Giri, and G. A. Worth, J. Chem. Phys. **129**, 174104 (2008).
[23] I. Yamazaki, T. Murao, T. Yamanaka, and K. Yoshimura, Faraday Discuss. Chem. Soc. **75**, 395 (1983).